International Journal of Solids and Structures 48 (2011) 208–216

Contents lists available at ScienceDirect

International Journal of Solids and Structures

journal homepage: www.elsevier.com/locate/ijsolstr

An improved numerical method for computation of stress intensity factors along 3D curved non-planar cracks in FGMs

Rahmatollah Ghajar [a,*], Ali Shaghaghi Moghaddam [a], Marco Alfano [b]

[a] Mechanical Properties Research Laboratory (MPRL), Department of Mechanical Engineering, K.N. Toosi University of Technology, Pardis St., Molasdra Ave., Vanak Sq., Tehran, Iran
[b] Department of Mechanical Engineering, University of Calabria, P. Bucci 44C, 87036 Arcavacata di Rende (CS), Italy

ARTICLE INFO

Article history:
Received 19 May 2010
Received in revised form 11 August 2010
Available online 25 September 2010

Keywords:
FGMs
Arbitrary curved non-planar crack
Stress intensity factors
Interaction integral

ABSTRACT

A simplified strategy based on the interaction energy integral is implemented in the finite element framework to evaluate mixed mode Stress Intensity Factors (SIFs) in 3D non-planar cracks. The proposed approach does not require any *a priori* information about crack front and crack surface curvatures, therefore different arbitrary non-planar cracks can be easily investigated. In particular, both conical and lens-shaped cracks in homogeneous materials are considered as case studies in order to demonstrate the accuracy of the present approach. Finally, the computational strategy is extended to Functionally Graded Materials (FGMs) and the effect of graded material properties (Young's modulus and Poisson's ratio) on the SIFs is studied in detail.

1. Introduction

The impact of a small hard object on the surface of brittle materials usually leads to the formation of ring cracks and to the occurrence of a conical fracture proceeding downward from the damaged area (Mencik, 1996). Conical cracks also arise in response to indentation loading (Gogotsi, 2009). Due to complexity of non-planar cracks, the analytical solutions for fracture parameters (e.g. SIFs) are limited to some special cases, and therefore additional studies for cracks of general curved shapes are needed. Sládek and Sládek (1983) derived boundary integral solutions to crack problems with cylindrical and spherical crack surfaces. Forth and Keat (1996) obtained some solutions to non-planar crack problems using the surface integral method. As an alterative, Chang and Wu (2007) computed mixed mode SIFs for 3D non-planar cracks by modifying the concept of the J_k and G_{III} integrals.

On the other hand, the interaction energy integral allows to make accurate and robust estimates of stress intensity factors. It is derived from the *J-integral* by considering a composition of two admissible states (Yau et al., 1980). In particular, converting the contour interaction integral to a finite domain surrounding the crack front, singular elements are removed from numerical computation (Nikishkov and Atluri, 1987). As a consequence, this approach does not require to accurately capture singular fields in the vicinity of crack tip, moreover, it can be easily introduced in the finite element context. Gosz and Moran (2002) adopted the interaction integral method to study 3D non-planar cracks in homogeneous materials. In order to define auxiliary fields at integration points for curved non-planar cracks, they employed a curvilinear coordinate system located at integration points. Recently Shaghaghi et al. (submitted for publication) successfully extended the procedure proposed by Gosz and Moran (2002) to 3D non-planar cracks in graded solids. Note that this topic was fairly unexplored because earlier works focused on 3D planar cracks only (Yu et al., 2010; Walters et al., 2004, 2006; Yildirim et al., 2005; Ayhan, 2009, 2007). However, it was observed in Gosz and Moran (2002) that by imposing auxiliary fields in curvilinear coordinate system the auxiliary strain field is not symmetric gradient of auxiliary displacement field and auxiliary stress field is not in equilibrium. Hence special care should be devoted to compensate the influence of crack curvature. For this reason, analytical equations for crack front and crack surface are required to find gradient of auxiliary displacement field, divergence of auxiliary stress field and location of integration points with respect to crack front. Although the previous method has been successfully applied to determine SIFs in homogeneous and FGM materials, in the finite element context it would be more convenient to develop a computational procedure which requires reduced *a priori* information regarding crack front and crack surface. In such a way any 3D non-planar cracks could be analyzed within the same numerical framework.

Therefore, the aim of the present work is to develop an improved technique, based on the interaction integral in domain form, for computation of mixed mode SIFs along 3D curved non-planar cracks. In addition, the proposed procedure will be also extended to graded materials. To demonstrate the

* Corresponding author. Tel.: +98 21 84063240.
E-mail address: Ghajar@kntu.ac.ir (R. Ghajar).

0020-7683/$ - see front matter © 2010 Elsevier Ltd. All rights reserved.
doi:10.1016/j.ijsolstr.2010.09.018

capabilities of the present approach, a conical crack in homogeneous material is firstly considered. The results obtained are in turn compared with those provided by ABAQUS. In order to assess the advantages introduced with respect to previous related methods, the conical crack is also analyzed using the approach proposed by Gosz and Moran (2002), Shaghaghi et al. (submitted for publication). To this aim the contribution of the different terms involved to account for the influence of crack curvature are compared. In addition, the case of a lens-shaped crack, for which an analytical solution for SIFs do exist, is also examined. Finally, both example are studied considering graded material properties and the influence of gradation of Young's modulus and Poisson's ratio on SIFs is investigated.

2. Interaction integral in domain form

Interaction energy integral is a two state integral which allows the stress intensity factor to be computed independently by superimposing suitable auxiliary fields to the actual fields. Actual fields are those obtained from finite element analysis and auxiliary fields are chosen to be asymptotic crack tip solutions Williams, 1957. So far this approach has been employed by several authors to study 2D and 3D planar cracks for homogeneous and graded materials Walters et al., 2005, 2006. In practice, it is more efficient to express the crack tip contour integral as a domain integral (Nikishkov and Atluri, 1987). This approach removes the need to precisely capture the details of the singular fields near the crack tip and also it is well suited to be implemented in the finite element context. For 3D non-planar cracks in homogeneous solids, Gosz and Moran (2002) proposed the interaction integral in domain form in conjunction with curvilinear coordinate systems.

Let us consider a point s along the front of an arbitrary shaped crack, as shown in Fig. 1(a). Following the works by Gosz and Moran (2002) the interaction integral over a finite domain V, neglecting the surface integrals, is given as:

$$J^{(1,2)}(s) = -\frac{1}{\gamma}\left[\int_V \left[\mathbf{tr}(\mathbf{H}^{(1,2)}\cdot\vec{\nabla}\mathbf{q}) + \vec{\nabla}\cdot\mathbf{H}^{(1,2)}\cdot\mathbf{q}\right]dV\right] \tag{1}$$

with

$$\gamma = \int_{-\frac{L_c}{2}}^{\frac{L_c}{2}} \Delta a(\xi)d\xi$$

where $\mathbf{q}$ is a sufficiently smooth vector field in V, $\Delta a(\xi)$ is the magnitude of the crack advance at crack front segment L_c and ξ represents coordinate along crack front, as shown in Fig. 1(b). Tensor $\mathbf{H}^{(1,2)}$ and its divergence in Cartesian coordinate system are given as follows:

$$H_{lj}^{(1,2)} = \sigma_{mn}^{(1)}\varepsilon_{mn}^{(2)}\delta_{lj} - \left(\sigma_{ij}^{(1)}u_{i,l}^{(2)} + \sigma_{ij}^{(2)}u_{i,l}^{(1)}\right) \tag{2}$$

$$H_{lj,j}^{(1,2)} = C_{mnpq}(\mathbf{X})_{,l}\varepsilon_{pq}^{(2)}\varepsilon_{mn}^{(1)} + \sigma_{mn}^{(1)}\left(\varepsilon_{mn}^{(2)} - u_{m,n}^{(2)}\right)_{,l} - \sigma_{mn,n}^{(2)}u_{m,l}^{(1)} \tag{3}$$

$C_{mnpq}(\mathbf{X})$ is the material constitutive tensor which is spatially varying for graded materials. Superscripts (1) and (2) refer to the actual and auxiliary fields, respectively. The interaction integral for 3D FGMs in Linear Elastic Fracture Mechanics (LEFM) is related to SIFs by the following equation (Walters et al., 2006):

$$J^{(1,2)}(s) = \frac{2(1-\nu(s)^2)}{E(s)}\left(K_I^{(1)}K_I^{(2)} + K_{II}^{(1)}K_{II}^{(2)}\right) + \frac{2(1+\nu(s))}{E(s)}K_{III}^{(1)}K_{III}^{(2)} \tag{4}$$

In Eq. (4) the quantities $\left(K_I^{(1)}, K_{II}^{(1)}, K_{III}^{(1)}\right)$ and $\left(K_I^{(2)}, K_{II}^{(2)}, K_{III}^{(2)}\right)$ refer to mixed mode SIFs for actual and auxiliary fields, respectively. $E = E(s)$ and $\nu = \nu(s)$ are Young's modulus and Poisson's ratio at crack front location s. In order to extract SIFs for actual state, i.e. $K_I^{(1)}$, the counterpart SIF for auxiliary state is set nonzero, i.e. $\left(K_I^{(2)} = 1; K_{II}^{(2)} = 0; K_{III}^{(2)} = 0\right)$, and then Eq. (4) yields:

$$K_I^{(1)} = \frac{E}{2(1-\nu^2)}J^{(1,2)}(s) \tag{5}$$

In what follows the numerical computation of interaction integral and SIFs is addressed.

3. Finite element implementation

In this work the finite element simulations are carried out using the finite element package ABAQUS. In particular isoparametric graded finite elements are implemented through the User Element (UEL) capabilities available in ABAQUS. The graded elements incorporates the material property gradient at the size scale of the element and it is based on the general framework proposed in Kim and Paulino (2002). Details on the implementation of the isoparametric graded finite element are provided in Shaghaghi et al. (2010b). In particular, it was shown that 20-noded brick elements with $2 \times 2 \times 2$ Gauss quadrature rule are well suited for modelling 3D FGMs. In the finite element setting, the finite domain V, over which the interaction integral is defined, represents some elements surrounding the crack tip at crack front location s. The point s coincides with a node in the finite element mesh. According to Fig. 2(a) this node may be either a midside node or a corner node. For the case of midside node, the finite domain V is assumed to have one element along the crack front and some rings of elements in radial direction, see Fig. 2(b). However for corner node two elements along the crack front are considered, see Fig. 2(c). The interaction integral can be now rewritten in reference to the above

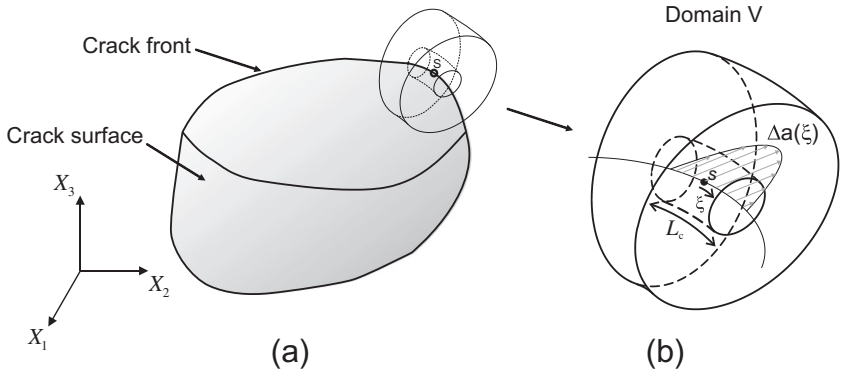

Fig. 1. (a) Finite domain V along curved non-planar crack; (b) variation of $\Delta a(\xi)$ along segment L_c at crack front.

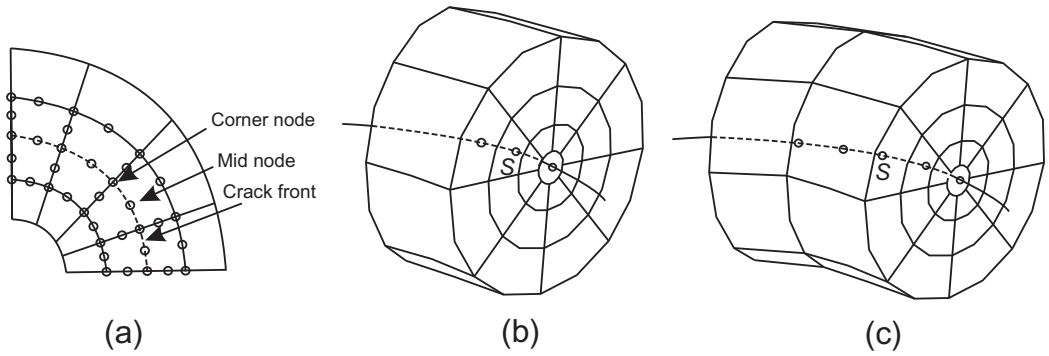

Fig. 2. Details of the finite element mesh corresponding to the finite domain V over which the domain integral is defined. (a) Cross section of the mesh for a generic finite domain (the dashed line represents the crack front); (b) finite domain when point s corresponds to a midside node and (c) to a corner node. Note that the effective number of rings of elements depend on the actual domain size.

mentioned finite domain V and considering the Gauss-quadrature scheme as follows:

$$\bar{J}(s) = \sum_{V=1}^{elems}\sum_{p=1}^{8}\left[\left(\sigma_{mn}^{(1)}\varepsilon_{mn}^{(2)}\delta_{lj} - \left(\sigma_{ij}^{(1)}u_{i,l}^{(2)} + \sigma_{ij}^{(2)}u_{i,l}^{(1)}\right)\right)q_{l,j}\right]_p \det\mathbf{J}\, w_p + \sum_{V=1}^{elems}\sum_{p=1}^{8}\left[\left(C_{mnpq}(\mathbf{X})_{,l}\varepsilon_{pq}^{(2)}\varepsilon_{mn}^{(1)} + \sigma_{mn}^{(1)}\left(\varepsilon_{mn}^{(2)} - u_{m,n}^{(2)}\right)_{,l} - \sigma_{mn,n}^{(2)}u_{m,l}^{(1)}\right)q_l\right]_p \det\mathbf{J}\, w_p \tag{6}$$

where the summation is done over the eight integration points pertaining to the elements included in domain V. Parameters w_p and $\det\mathbf{J}$ denote the corresponding weight for integration points and determinant of the coordinate Jacobian matrix, respectively. Actual fields are the solution of finite element analysis in ABAQUS. Therefore to compute Eq. (6) it is required to define auxiliary fields as well as the components of vector field $\mathbf{q}$ and their derivatives $q_{l,j}$ at integration points. Note that all quantities in Eq. (6) are defined with respect to a fixed Cartesian coordinate system. In what follows the definition of auxiliary fields and vector $\mathbf{q}$ are addressed to evaluate Eq. (6).

3.1. Constructing auxiliary fields

Gosz and Moran (2002) studied the SIFs for 3D non-planar cracks in homogeneous materials and, in order to set-up auxiliary fields at integration points, a curvilinear coordinate system was employed. In particular, auxiliary fields were constructed considering Williams solution for 2D asymptotic fields in the vicinity of a crack. However, it was observed in Gosz and Moran (2002), that by imposing auxiliary fields in curvilinear coordinate system the auxiliary strain field is not symmetric gradient of auxiliary displacement field and auxiliary stress field is not in equilibrium. Therefore, much attention must be paid to compensate the influence of crack curvature. It was shown that analytical equations for crack front and crack surface are required to find gradient of auxiliary displacement field, divergence of auxiliary stress field as well as to locate integration points with respect to crack front. However, Walters et al. (2005) observed that the values of r and θ computed using the above mentioned analytical equations can yield incorrect position of integration points if the analytical crack front extends to some rings of elements. This problem leads to auxiliary-fields inconsistent with actual fields generated by the finite element mesh. For this reason, in studying general 3D non-planar cracks, it would be beneficial to locate position of integration points based on finite element mesh and regardless of analytical equations for crack front and crack surface. For this reason, in the present work a procedure able to locate integration points with respect to crack front for 3D non-planar crack has been developed. In particular, the procedure is an extension of the work proposed by Walters et al. (2005) for 3D planar cracks.

The node s on crack front in Fig. 3(a) represents a midnode to compute SIFs. The procedure requires a local coordinate system at this point with unit basis $\bar{\mathbf{e}}_i$ and coordinates $x_i (i = 1,2,3)$. The unit basis $\bar{\mathbf{e}}_3$ and $\bar{\mathbf{e}}_2$ are directed toward the tangent vector to the crack front and normal vector to the crack surface at point s, respectively. Finally, the unit basis $\bar{\mathbf{e}}_1$ is chosen so that a right-handed coordinate system is formed. Note that for all approaches based on *J-integral*, it is required to set up unit basis $\bar{\mathbf{e}}_1$. In Fig. 3(a) the integration point p and two neighboring nodes a and b are also depicted. Consider the case in which the integration point p is on the left side of node s, let's say close to node a. Now draw a vector with starting point at node s and ending point at node a, $\vec{sa}$. Then construct a plane with normal $\hat{\mathbf{n}}$ where:

$$\hat{\mathbf{n}} = \frac{\bar{\mathbf{e}}_1 \times \vec{sa}}{\|\vec{sa}\|} \tag{7}$$

The integration point p is now projected to this plane, point p'. The minimum distance between point p' and edge sa is given as:

$$p'M = \frac{\left\|\vec{sp'} \times \vec{sa}\right\|}{\|\vec{sa}\|} \tag{8}$$

where M represents a location on edge sa closest to point p'. From Fig. 3(b) it is concluded that $r = \sqrt{(p'M)^2 + (pp')^2}$. Actual fields obtained by FE analysis at the upper and lower surfaces of crack faces are discontinuous. The auxiliary fields have to capture these discontinuities in order to ensure consistency with actual fields at crack surfaces. Hence the major issue for the accurate computation of θ arises because of the discontinuities on auxiliary fields at $\theta = \pm 180°$. In the present work, the Fortran command *ATAN2*() was used in order to differentiate between quadrants. In quadrants I and II θ varies between 0° and 180° and in quadrants *III* and *IV* the range of θ is $[0 \sim -180]°$, see Fig. 3(c). Therefore θ has been evaluated as *ATAN2* (PP',$P'M$). Having defined r and θ, the auxiliary displacement, $\bar{\mathbf{u}}^{(2)}$, and the auxiliary strain fields, $\bar{\boldsymbol{\varepsilon}}^{(2)}$, in local coordinate system are given as:

$$\bar{u}_j^{(2)} = \frac{K_I^{(2)}}{2\mu}\sqrt{\frac{r}{2\pi}}g_j^I(\theta,\nu) + \frac{K_{II}^{(2)}}{2\mu}\sqrt{\frac{r}{2\pi}}g_j^{II}(\theta,\nu) + \frac{K_{III}^{(2)}}{2\mu}\sqrt{\frac{r}{2\pi}}g_j^{III}(\theta,\nu) \tag{9}$$

$$\bar{\varepsilon}_{ij}^{(2)} = \frac{1}{2}\left(\frac{\partial\bar{u}_i^{(2)}}{\partial x_j} + \frac{\partial\bar{u}_j^{(2)}}{\partial x_i}\right) \tag{10}$$

where $g_j(\theta,\nu)$ is the angular function (Walters et al., 2006). In the case of FGMs we should compensate the effect of material

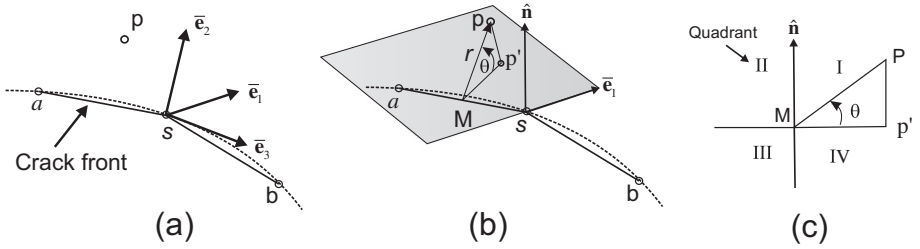

Fig. 3. (a) Local coordinate system at mid node; (b) details on the computation of r and θ; (c) schematic depiction of the quadrants I–IV.

gradation. In this work the auxiliary stress field is related to the auxiliary strain field through the constitutive tensor as:

$$\bar{\sigma}_{ij}^{(2)} = C_{ijkl}(\mathbf{X})\bar{\varepsilon}_{kl}^{(2)} \tag{11}$$

To be consistent with actual fields, the auxiliary fields are transformed to Cartesian coordinate system. Through the use of a transformation tensor, $\mathbf{Q}$, the auxiliary stress, strain and displacement fields, $(\boldsymbol{\sigma},\boldsymbol{\varepsilon},\mathbf{u})$, are given by:

$$\begin{aligned}\boldsymbol{\varepsilon} &= \mathbf{Q}^T\bar{\boldsymbol{\varepsilon}}\mathbf{Q}\\ \boldsymbol{\sigma} &= \mathbf{Q}^T\bar{\boldsymbol{\sigma}}\mathbf{Q}\\ \boldsymbol{u} &= \mathbf{Q}^T\bar{\boldsymbol{u}}\end{aligned} \tag{12}$$

As the auxiliary fields are now referred to a fix local coordinate system, it is observed that strain–displacement compatibility is satisfied and auxiliary stress field satisfies equilibrium. Therefore for homogenous solids the terms $\sigma_{mn,n}^{(2)}$ and $\left(\varepsilon_{mn}^{(2)} - u_{m,n}^{(2)}\right)$ in Eqs. (3) and (6) vanish. Note that for a spatially varying constitutive tensor (graded material properties) the auxiliary stress field is not in equilibrium and has to be considered.

3.2. Evaluating $\boldsymbol{q}$ function

Fig. 4(a) shows the finite domain V when point s, at crack front, coincides with a midside node. Specifically, the domain V spans one element in the finite element mesh. Let consider a cross section of the domain V in the $\bar{\mathbf{e}}_1 - \bar{\mathbf{e}}_3$ plane, see Fig. 4(b). We denote $\Delta a(\xi)$ the values of the $\bar{\boldsymbol{q}}$ function along crack front segment L_c (in the $\bar{\mathbf{e}}_1$-direction). The value of $\bar{\boldsymbol{q}}$ for the nodes indicated by ∘ is zero and the value is unity for the nodes indicated by •. As a consequence, for an element pertaining to the finite domain V, the $\bar{\boldsymbol{q}}$ function at a generic node a, with respect to a local coordinate system, is given as:

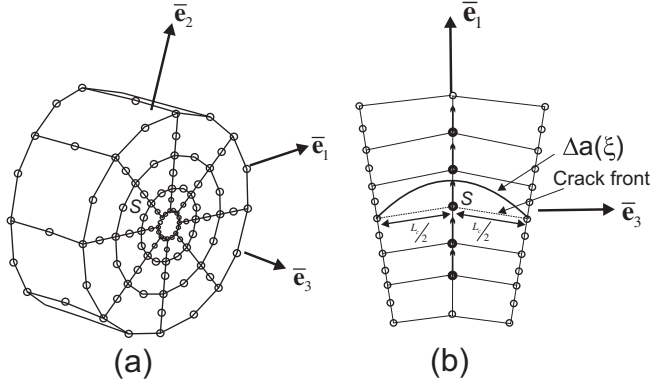

Fig. 4. (a) Finite element discretization of domain V in the case of midside node; (b) variation of the $\mathbf{q}$-function along the crack front segment L_c.

$$\bar{q}_l^a = \begin{cases} = 0 & \text{for nodes on the boundary of domain } V\\ = \bar{\mathbf{e}}_1 & \text{for inner nodes}\end{cases} \tag{13}$$

where $\bar{q}_l^a$ is the components of $\bar{\boldsymbol{q}}$ at node a in local coordinate system. Then vector $\bar{\boldsymbol{q}}$ is transformed to Cartesian coordinate system, $\boldsymbol{q}$, as follows:

$$\boldsymbol{q} = Q^T\bar{\boldsymbol{q}} \tag{14}$$

Consistent with isoparametric finite element formulation, q_l and $q_{l,j}$ at integration points in Cartesian system are interpolated as follows:

$$\begin{aligned} q_l &= \sum_{a=1}^{20} N_a q_l^a\\ q_{l,j} &= \sum_{a=1}^{20} N_{a,j} q_l^a\end{aligned} \tag{15}$$

The shape of the $\Delta a(\xi)$ at crack front segment L_c for a midside node basically does not contribute to the computation of q_l and $q_{l,j}$ at integration points. The shape of the $\Delta a(\xi)$ only affects the integrand γ in Eq. (1). Let's consider for $\Delta a(\xi)$ the following form:

$$\Delta a(\xi) = 1 - \left|\frac{2}{L_c}\xi\right|^c \tag{16}$$

$\Delta a(\xi)$ stands for a quadratic shape when $c = 2$ (Nikishkov and Atluri, 1987). In this work, by examining several problems, it was observed that value of 2.06 for c provides accurate results. This value is taken constant for all the problems considered here. The integrand γ in Eq. (1) is then evaluated as:

$$\gamma = \int_{-\frac{L_c}{2}}^{\frac{L_c}{2}} \Delta a(\xi) d\xi = 1.01 \times \frac{2}{3} L_c \tag{17}$$

For the finite domain V over two elements at corner node a similar approach is implemented.

3.3. Accounting for graded material properties

For graded materials the terms including derivatives of material constitutive tensor, $C_{mnpq}(\mathbf{X})_{,l}$, in Eq. (6) contributes to the interaction integral. For isotropic elastic FGMs, the constitutive tensor is given as:

$$C_{mnpq}(\mathbf{X}) = \lambda(\mathbf{X})\delta_{mn}\delta_{pq} + \mu(\mathbf{X})(\delta_{mp}\delta_{nq} + \delta_{mq}\delta_{np}) \tag{18}$$

where δ_{mn} is the Kronecker delta, and $\mu(\mathbf{X})$ and $\lambda(\mathbf{X})$ are spatially varying Lame' constants defined as follows:

$$\lambda(\mathbf{X}) = \frac{E(\mathbf{X})\nu(\mathbf{X})}{(1+\nu(\mathbf{X}))(1-2\nu(\mathbf{X}))}, \quad \mu(\mathbf{X}) = \frac{E(\mathbf{X})}{2(1+\nu(\mathbf{X}))} \tag{19}$$

$E(\mathbf{X})$ and $\nu(\mathbf{X})$ are spatially varying Young's modulus and Poisson's ratio, respectively. The derivative of constitutive tensor in Cartesian coordinate system is given as:

$$C_{mnpq}(\mathbf{X})_{,l} = \frac{\partial C_{mnpq}(\mathbf{X})}{\partial E(\mathbf{X})}\frac{\partial E(\mathbf{X})}{\partial X_l} + \frac{\partial C_{mnpq}(\mathbf{X})}{\partial \nu(\mathbf{X})}\frac{\partial \nu(\mathbf{X})}{\partial X_l}, \quad l = 1,2,3 \tag{20}$$

where

$$\frac{\partial C_{mnpq}(\mathbf{X})}{\partial E(\mathbf{X})} = \frac{1}{E(\mathbf{X})} C_{mnpq}(\mathbf{X}) \tag{21}$$

$$\frac{\partial C_{mnpq}(\mathbf{X})}{\partial \nu(\mathbf{X})} = \frac{E(\mathbf{X})(1+2\nu(\mathbf{X})^2)}{[(1+\nu(\mathbf{X}))(1-2\nu(\mathbf{X}))]^2}\delta_{mn}\delta_{pq} - \frac{E(\mathbf{X})}{2(1+\nu(\mathbf{X}))^2}(\delta_{mp}\delta_{nq}+\delta_{mq}\delta_{np}) \tag{22}$$

In the finite element formulation, material properties and their derivatives at integration points are computed using isoparametric interpolations (Li and Zou, 1998):

$$\nu(\mathbf{X}) = \sum_{I=1}^{20} \nu_I N_I, \quad \frac{\partial \nu(\mathbf{X})}{\partial X_l} = \sum_{I=1}^{20} \nu_I \frac{\partial N_I}{\partial X_l}$$
$$E(\mathbf{X}) = \sum_{I=1}^{20} E_I N_I, \quad \frac{\partial E(\mathbf{X})}{\partial X_l} = \sum_{I=1}^{20} E_I \frac{\partial N_I}{\partial X_l} \tag{23}$$

where E_I and ν_I are nodal values of the elastic properties and N_I are shape functions.

4. Numerical examples

The procedure outlined in the previous sections is now employed to compute mixed-mode SIFs along 3D non-planar cracks. A conical crack is investigated to assess the capability of the present approach for non-planar cracks. It is worth noting that this problem geometry was also analyzed in ABAQUS[1] (Hibbitt et al., 2006). Furthermore a lens shaped crack is also considered to study the influence of mesh refinement on the results.

4.1. Conical crack

Fig. 5 shows the problem of a conical crack in an infinite solid half-space. The crack circumscribes a circle with a radius of 10 length units on the free surface and intersects the free surface at 45° and extends 15 length units into the solid domain. The applied load is a static pressure with a magnitude of 10 force/length^2 applied on the circular free surface of the block circumscribed by the crack. The linear static structural analysis requires specification of Young's modulus, which is 30,000,000 units of force/length^2, and Poisson's ratio, which is 0.3. Although the geometry and loading condition are axisymmetric, the 3D model is investigated here to demonstrate the capability of the present approach. The input file employed for the simulation was retrieved from ABAQUS. The corresponding 3D domain discretized using 3D brick elements is shown in Fig. 6(a). The mesh represents a quarter-symmetric segment of the problem domain with 9517 20-noded brick element and 42,089 nodes. To minimize the influence of curvature on the results and to obtain domain-independent results, a very refined mesh was employed in ABAQUS; in particular 18 elements were inserted along crack front and the crack is surrounded by 16 sectors of elements as shown in Fig. 6(b). Elements at crack front have quarter-point nodes and collapsed faces and are of size $L_e/a = 1/50$, with L_e being the size of elements incident at the crack front.

The values of K_I, K_{II} and *J-integral* at a location halfway the crack front obtained from this FE model are reported in ABAQUS (Hibbitt et al., 2006). The domain independency of the results is assessed by evaluating fracture parameters in four domains each corresponding to the ring of elements taken outward radially from the crack tip. While there is no analytical solution available for comparison, ABAQUS reported the results obtained from an axisymmetric analysis with extreme mesh refinement as reference (these values are reported in parentheses in Table 1). This example is considered herein as a case of study to obtain fracture parameters using the present approach. The results are tabulated in Table 1.

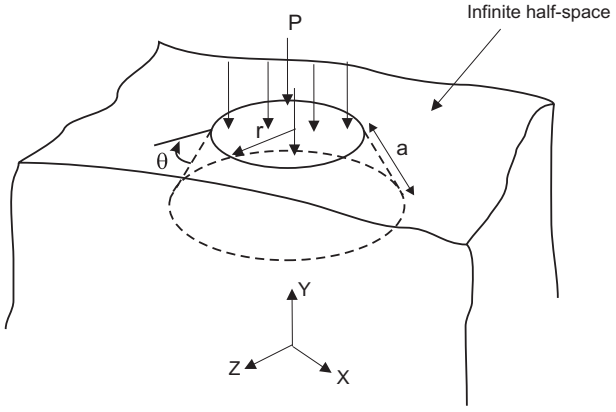

Fig. 5. Schematic depiction of a conical crack in an infinite solid half-space.

The results obtained using the present approach are in good agreement with the reference values that are shown in parenthesis. Moreover, results accuracy and domain independency are higher than those obtained using ABAQUS. Gosz and Moran (2002) employed curvilinear coordinate system to construct auxiliary field along curved cracks. They emphasized the importance of including extra terms in domain integral to account for the influence of crack curvature. Otherwise the domain integral would be domain dependant. In the present approach a local coordinate system, fixed on crack front, is employed to define auxiliary fields. To examine the contribution of the extra terms in domain integral, the conical crack is studied considering (1) curvilinear coordinate system, CCS, and (2) local coordinate system, LCS. The interaction integral can be rewritten as follows:

$$\begin{aligned}
J^{(1,2)}(s) &= J_1^{(1,2)}(s) + J_2^{(1,2)}(s) + J_3^{(1,2)}(s) + J_4^{(1,2)}(s)\\
J_1^{(1,2)}(s) &= -\frac{1}{\gamma}\int_V \left[\sigma_{mn}^{(1)}\varepsilon_{mn}^{(2)}\delta_{lj} - \left(\sigma_{ij}^{(1)}u_{i,l}^{(2)} + \sigma_{ij}^{(2)}u_{i,l}^{(1)}\right)\right]dV\\
J_2^{(1,2)}(s) &= -\frac{1}{\gamma}\int_V \left[C_{mnpq}(\mathbf{X})_{,l}\varepsilon_{pq}^{(2)}\varepsilon_{mn}^{(1)}q_l\right]dV\\
J_3^{(1,2)}(s) &= -\frac{1}{\gamma}\int_V \left[\sigma_{mn}^{(1)}\left(\varepsilon_{mn}^{(2)} - u_{m,n}^{(2)}\right)_{,l}q_l\right]dV\\
J_4^{(1,2)}(s) &= -\frac{1}{\gamma}\int_V \left[-\sigma_{mn,n}^{(2)}u_{m,l}^{(1)}q_l\right]dV
\end{aligned} \tag{24}$$

The term $J_2^{(1,2)}(s)$ contributes in the case of graded material properties only. For homogeneous materials, the terms $J_3^{(1,2)}(s)$ and $J_4^{(1,2)}(s)$ reflect the influence of crack curvature. Stress intensity factors are computed here with both approaches by considering and neglecting the extra terms as:

$$\begin{aligned}
K_m^{(1)}|_1 &= \frac{E(s)}{2(1-\nu(s)^2)}J_1^{(1,2)}(s)\\
K_m^{(1)}|_2 &= \frac{E(s)}{2(1-\nu(s)^2)}\left[J_2^{(1,2)}(s) + J_3^{(1,2)}(s) + J_4^{(1,2)}(s)\right]\\
K_m^{(1)} &= K_m^{(1)}|_1 + K_m^{(1)}|_2
\end{aligned} \tag{25}$$

where $m = I$ and II. The results are tabulated in Table 2. It is clear that in $K_I^{(1)}|_2$ the terms $J_3^{(1,2)}(s) + J_4^{(1,2)}(s)$ must be included for the numerical computation of domain integrals using curvilinear coordinate system to ensure accuracy and domain independency. However these terms vanish when local coordinate system is employed. Thereby the present approach provides accurate results with less computation costs and prior efforts.

[1] ABAQUS 6.7 example library.

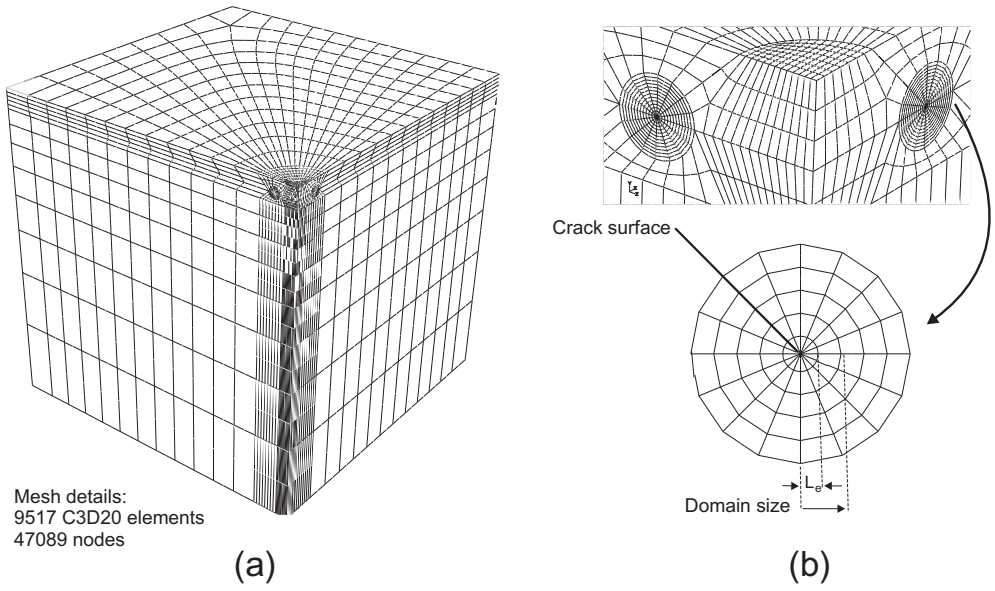

Fig. 6. Details of the finite element model of a conical crack. (a) 3D mesh employed to model the conical crack; (b) details of the finite element mesh at crack tip.

Table 1
Comparison of present approach with Abaqus.

Fracture parameters	Approach	Domain1	Domain2	Domain3	Domain4
K_I(=0.491)	Present	0.492	0.494	0.493	0.493
	Abaqus	0.501	0.503	0.502	0.500
K_{II}(=2.03)	Present	2.021	2.022	2.023	2.024
	Abaqus	2.029	2.018	2.004	1.987
J(=1.33)($\times 10^{-7}$)	Present	1.337	1.338	1.339	1.338
	Abaqus	1.334	1.336	1.337	1.337

Table 2
Values obtained for SIFs considering curvilinear (CCS) and local (LCS) coordinate systems.

SIFs	Approach	Components	Domain1	Domain2	Domain3	Domain4
K_I(=0.491)	LCS	$K_I^{(1)}\|_1$	0.492	0.493	0.493	0.493
		$K_I^{(1)}\|_2$	0.000	0.000	0.000	0.000
		$K_I^{(1)}$	0.492	0.493	0.493	0.493
	CCS	$K_I^{(1)}\|_1$	0.489	0.485	0.481	0.476
		$K_I^{(1)}\|_2$	0.003	0.007	0.012	0.016
		$K_I^{(1)}$	0.492	0.492	0.493	0.492
K_{II}(=2.03)	LCS	$K_{II}^{(1)}\|_1$	2.021	2.023	2.023	2.024
		$K_{II}^{(1)}\|_2$	0.000	0.000	0.000	0.000
		$K_{II}^{(1)}$	2.021	2.023	2.023	2.024
	CCS	$K_{II}^{(1)}\|_1$	2.021	2.016	2.010	2.003
		$K_{II}^{(1)}\|_2$	0.006	0.011	0.017	0.024
		$K_{II}^{(1)}$	2.027	2.027	2.027	2.027

The stress intensity factors are now examined for a conical crack embedded in a graded solids using the present approach. Elastic properties are assumed to vary exponentially in Y direction to a depth $y_2 = 20$ as shown in Fig. 7. Specifically:

$$E(y) = E_{ct} e^{\beta(y-y_c)}, \quad \beta = -\frac{1}{y_2}\ln\left(\frac{E_1}{E_2}\right)$$
$$\nu(y) = \nu_{ct} e^{\beta'(y-y_c)}, \quad \beta' = -\frac{1}{y_2}\ln\left(\frac{\nu_1}{\nu_2}\right) \tag{26}$$

where β and β' are gradation indexes and y_c denotes the Y coordinate of crack front. E_{ct} and ν_{ct} represent the values of elastic properties at

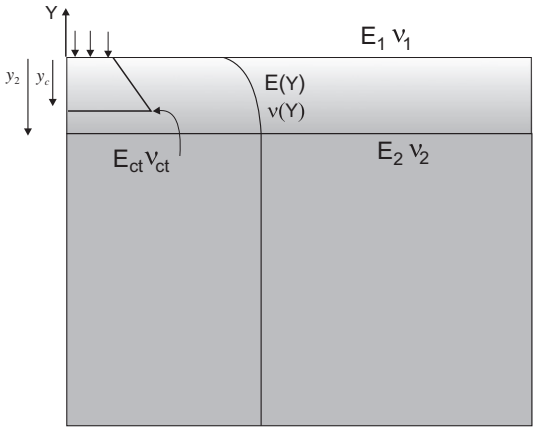

Fig. 7. Material gradation profile for a conical crack in an infinite solid half-space.

crack tip. Tables 3 and 4 illustrate the interaction integral components for $K_I^{(1)}$ and $K_{II}^{(1)}$ with respect to different values of E_1/E_2. Poisson's ratio is taken constant 0.3. It can be seen from Tables 3 and 4 that for $E_1/E_2 = 1$ only term $J_1^{(1,2)}(s)$ contributes to interaction integral in determining $K_I^{(1)}$ and $K_{II}^{(1)}$. The values of SIFs depend on material gradation and domain size. For $K_I^{(1)}$ the contribution of term $J_4^{(1,2)}(s)$ is superior to the contribution of $J_2^{(1,2)}(s)$. However for $K_{II}^{(1)}$ this trend is inverted. It is also inferred that, for any gradation index, the interaction integral remains basically domain independent.

The trend of stress intensity factors versus different E_1/E_2 is shown in Fig. 8. Poisson's ratio is taken constant and equal to 0.3. The same calculation is carried out for graded Poisson's ratio and constant modulus of elasticity, $E = 3e7$. Fig. 9 depicts the trend of SIFs versus different ν_1/ν_2. It is concluded that SIFs depend on gradation of material properties. By increasing E_1/E_2 both $K_I^{(1)}$ and $K_{II}^{(1)}$ increase. However when ν_1/ν_2 increases $K_{II}^{(1)}$ increases and $K_I^{(1)}$ decreases.

4.2. Lens shaped crack

Fig. 10(a) illustrates a cylinder of radius r and height H with an embedded lens-shaped crack whose surface geometry is

Table 3
Components of interaction integral ($\times 10^{-8}$) for $K_I^{(1)}$.

$\frac{E_1}{E_2}$	Domain	$J_1^{(1,2)}(s)$	$J_2^{(1,2)}(s)$	$J_3^{(1,2)}(s)$	$J_4^{(1,2)}(s)$	$J^{(1,2)}(s)$	$K_I^{(1)}$
0.5	1	0.758	0.003	0.000	−0.042	0.719	0.099
	2	0.845	0.011	0.000	−0.139	0.717	0.099
	3	0.949	0.022	0.000	−0.254	0.717	0.099
	4	1.065	0.035	0.000	−0.383	0.717	0.099
0.75	1	2.294	0.000	0.000	−0.019	2.275	0.313
	2	2.339	0.001	0.000	−0.065	2.276	0.313
	3	2.391	0.003	0.000	−0.119	2.275	0.313
	4	2.448	0.007	0.000	−0.180	2.275	0.313
1	1	3.579	0.000	0.000	0.000	3.579	0.492
	2	3.582	0.000	0.000	0.000	3.582	0.493
	3	3.582	0.000	0.000	0.000	3.582	0.493
	4	3.583	0.000	0.000	0.000	3.583	0.493
1.5	1	5.702	0.004	0.000	0.034	5.740	0.789
	2	5.623	0.010	0.000	0.113	5.746	0.790
	3	5.526	0.014	0.000	0.207	5.746	0.790
	4	5.417	0.016	0.000	0.313	5.746	0.790
2	1	7.451	0.010	0.000	0.064	7.524	1.035
	2	7.296	0.027	0.000	0.210	7.533	1.036
	3	7.108	0.040	0.000	0.386	7.534	1.036
	4	6.899	0.049	0.000	0.585	7.534	1.036

Table 4
Components of interaction integral ($\times 10^{-8}$) for $K_{II}^{(1)}$.

$\frac{E_1}{E_2}$	Domain	$J_1^{(1,2)}(s)$	$J_2^{(1,2)}(s)$	$J_3^{(1,2)}(s)$	$J_4^{(1,2)}(s)$	$J^{(1,2)}(s)$	$K_{II}^{(1)}$
0.5	1	12.635	−0.071	0.000	0.016	12.580	1.730
	2	12.770	−0.216	0.000	0.039	12.594	1.732
	3	12.908	−0.364	0.000	0.054	12.598	1.732
	4	13.054	−0.516	0.000	0.063	12.601	1.733
0.75	1	13.784	−0.032	0.000	0.006	13.759	1.892
	2	13.855	−0.098	0.000	0.016	13.774	1.894
	3	13.921	−0.164	0.000	0.021	13.778	1.894
	4	13.990	−0.232	0.000	0.023	13.781	1.895
1	1	14.697	0.000	0.000	−0.001	14.696	2.021
	2	14.715	0.000	0.000	−0.002	14.712	2.023
	3	14.720	0.000	0.000	−0.003	14.717	2.024
	4	14.723	0.000	0.000	−0.003	14.720	2.024
1.5	1	16.122	0.053	0.000	−0.014	16.162	2.222
	2	16.050	0.161	0.000	−0.031	16.180	2.225
	3	15.953	0.270	0.000	−0.038	16.185	2.225
	4	15.846	0.380	0.000	−0.038	16.188	2.226
2	1	17.230	0.097	0.000	−0.024	17.304	2.379
	2	17.082	0.294	0.000	−0.053	17.324	2.382
	3	16.899	0.493	0.000	−0.063	17.329	2.383
	4	16.699	0.694	0.000	−0.060	17.332	2.383

characterized by radius R and angle α. In particular the geometric parameters of the model are given as follows: $2r/H = 1$, $2r/R = 10$, $R = 1$ and $\alpha = \pi/4$. The values of elastic parameters employed in the simulations are $E = 68.9$ GPa and $\nu = 0.22$. Analytical solutions (Martynenko and Ulitko, 1978) and numerical data (Gosz and Moran, 2002) for SIFs are available for this problem geometry. Gosz and Moran (2002) used a finite element mesh in which the characteristic length of the smallest elements near the tip is $R/500$. They achieved accuracy with a maximum error of 0.3% for $K_I^{(1)}$ and 5% for $K_{II}^{(1)}$. For this crack Moës et al. (2002) used coarse mesh with the characteristic length of the smallest elements near the tip as $R/20$ and reported the values of SIFs with 2% error for $K_I^{(1)}$ and 10% for $K_{II}^{(1)}$. In practice it is of interest to have acceptable results with less computation

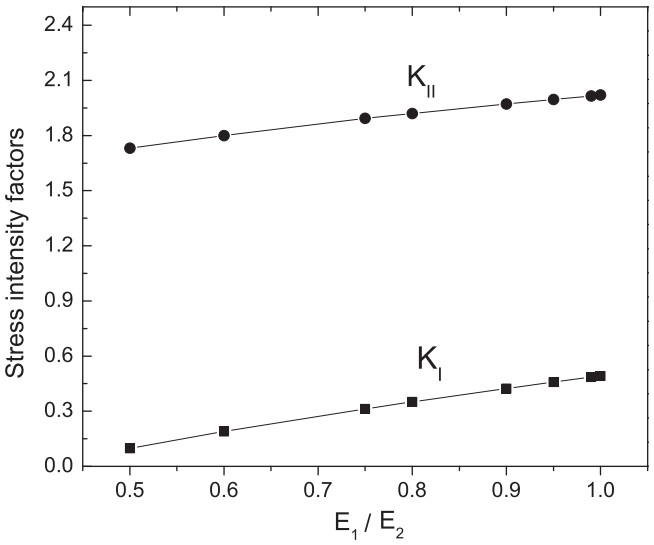

Fig. 8. SIFs versus E_1/E_2 for a conical crack in an infinite solid half-space.

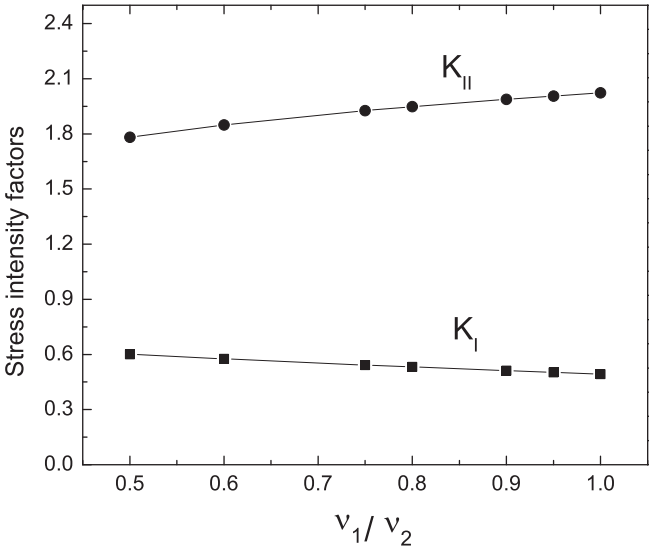

Fig. 9. SIFs versus ν_1/ν_2 for a conical crack in an infinite solid half-space.

costs. Here it is intended to study the influence of mesh size and number of element along crack front on SIFs. Here the local coordinate system is employed. Fig. 10(b) shows the finite element discretization of the lens shaped crack. The percent error of $K_I^{(1)}$ and $K_{II}^{(1)}$ with respect to analytical solution provided by Martynenko and Ulitko (1978) are tabulated in Table 5 for different L_e and n_{cf}. L_e refers to the size of the smallest element incident at crack front, n_{cf} refers to the number of element at crack front. The reference values are 0.877 and 0.235 for $K_I^{(1)}$ and $K_{II}^{(1)}$, respectively. It is inferred that even for a coarse mesh ($L_e = 0.04$) the error for $K_I^{(1)}$ is less than 1.6% and for $K_{II}^{(1)}$ less than 4%. By reducing the L_e, more accuracy is achieved. However the variation is negligible with respect to n_{cf}. Now we define J_K and J_A where J_K denotes the J values estimated from stress intensity factors and J_A denotes the J values estimated directly from *J-integral*. The ratio J_k/J_A for all cases deviates from unity 1.1% which is a good check for numerical computation of interaction integral.

The effect of graded material properties on the SIFs of a lens shaped crack in considered next. To this aim, the finite element discretization consists of 10 elements along crack front and $L_e = 0.015$;

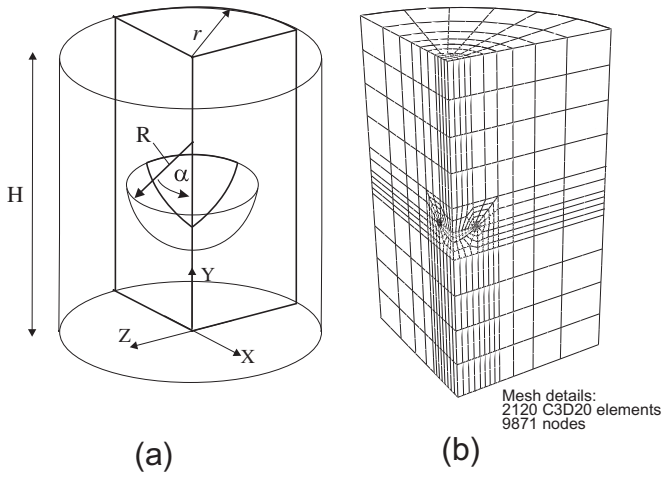

Fig. 10. (a) Characteristic geometrical features of the lens shaped crack; (b) corresponding finite element mesh developed in ABAQUS.

Table 5
Influence of mesh refinement on SIFs. The percentage of error for $K_I^{(1)}$ and $K_{II}^{(1)}$ are shown.

L_e	n_{cf}	Element	Node	$K_I^{(1)}$	$K_{II}^{(1)}$	$\frac{J_K}{J_A}$
0.04	6	1182	5763	1.4	2.9	0.992
	8	1632	7729	1.6	3.2	0.994
	10	2120	9871	1.5	3.3	0.994
0.025	6	1404	6822	0.9	3.4	0.991
	8	1728	8187	1.0	3.6	0.992
	10	2240	10,419	1.1	3.7	0.992
0.015	6	1476	7166	0.6	3.5	0.990
	8	1824	8621	0.8	3.7	0.991
	10	2360	10,967	0.8	3.9	0.991
0.01	8	1920	9079	0.6	3.8	0.990
	10	2480	11,515	0.7	4.0	0.991
0.005	12	2808	12,934	0.5	3.4	0.991
0.0025	14	3395	16,260	0.5	3.5	0.990

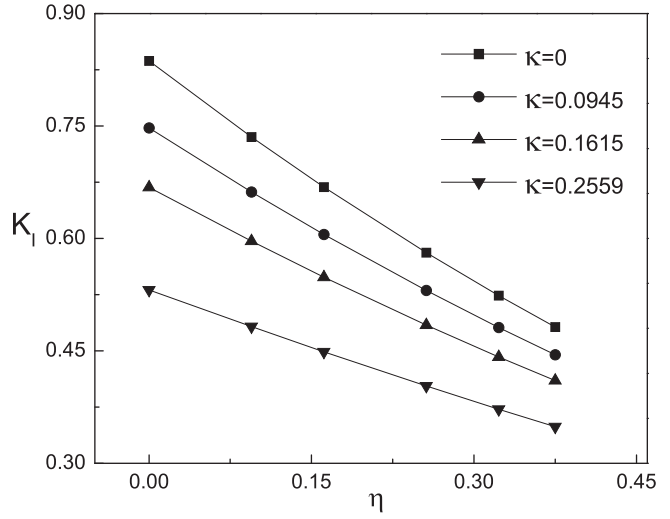

Fig. 11. Variation of K_I with respect to gradation indexes for Young's modulus and Poisson's ratio.

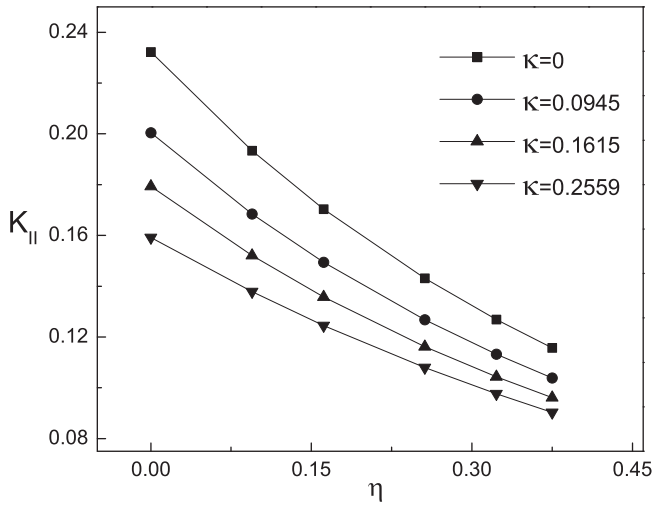

Fig. 12. Variation of K_{II} with respect to gradation indexes for Young's modulus and Poisson's ratio.

a total of 2360 elements has been employed for the model. Furthermore, exponential gradation in radial direction of both Young's modulus and Poisson's ratio are considered as follows:

$$E(r) = E_L e^{\eta r}, \quad \eta = \frac{1}{R} Ln\left(\frac{E_R}{E_L}\right)$$
$$\nu(r) = \nu_L e^{\kappa r}, \quad \kappa = \frac{1}{R} Ln\left(\frac{\nu_R}{\nu_L}\right) \tag{27}$$

where η and κ are gradation indexes for Young's modulus and Poisson's ratio and $r = \sqrt{X^2 + Z^2}$. Note that E_L and ν_L denote the values assumed by the elastic properties on the axis of symmetry ($r = 0$), while E_R and ν_R represent the corresponding values at the outer surface of the cylinder ($r = R$). The numerical computations have been carried out considering different values of the gradation indexes. The so obtained values of the mixed mode stress intensity factors are reported in Figs. 11 and 12. Based on these results it is inferred that material gradation do affect SIFs. Indeed, for this problem geometry, we observe that the SIFs decrease if gradation indexes increase.

5. Conclusion

In this work the interaction integral method was employed to extract stress intensity factors along 3D non-planar cracks. In particular, in the present approach a fixed local coordinate system was employed to define auxiliary fields. It was shown that by using a fixed local coordinate system located at crack front some extra terms embedded in the interaction integral can be neglected as they do not provide contribution to the SIFs. However, when curvilinear coordinate system is employed, these terms should be included to ensure accuracy and domain independency of interaction integrals. The evaluation of these extra terms requires analytical equations for crack front and surface. In the present approach, the locations of integration points can be determined without the need to know the analytical equations for crack front and crack surface. Therefore reduced computational efforts are required in the determination of the interaction integral. The proposed approach has been validated comparing the results obtained for 3D non-planar conical and lens-shaped cracks with the corresponding reference solutions. Finally, the influence of material gradation on SIFs was investigated and it was shown that SIFs depend on gradation of both Young's modulus and Poisson's ratio.

References

Ayhan, A.O., 2009. Three-dimensional mixed-mode stress intensity factors for cracks in functionally graded materials using enriched finite elements. International Journal of Solids and Structures 46 (3–4), 796–810.

Ayhan, A.O., 2007. Stress intensity factors for three-dimensional cracks in functionally graded materials using enriched finite elements. International Journal of Solids and Structures 44 (25–26), 8579–8599.

Chang, J.H., Wu, D.J., 2007. Stress intensity factor computation along a non-planar curved crack in three dimensions. International Journal of Solids and Structures 44 (2), 371–386.

Forth, S.C., Keat, W.D., 1996. Three-dimensional non-planar fracture model using the surface integral method. International Journal of Fracture 77 (3), 243–262.

Gosz, M., Moran, B., 2002. An interaction energy integral method for computation of mixed-mode stress intensity factors along non-planar crack fronts in three dimensions. Engineering Fracture Mechanics 69 (3), 299–319.

Gogotsi, G.A., 2009. Fracture behaviour of Mg-PSZ ceramics: comparative estimates. Ceramics International 35 (7), 2735–2740.

Hibbitt, Karlsson, Sorensen, Inc., 2006. ABAQUS/standard users manual, v. 6.7. Pawtucket, Rhode Island.

Kim, J.-H., Paulino, G.H., 2002. Isoparametric graded finite elements for nonhomogeneous isotropic and orthotropic materials. ASME Journal of Applied Mechanics 69, 502–514.

Li, C., Zou, Z., 1998. Stress intensity factors for a functionally graded material cylinder with an external circumferential crack. Fatigue and Fracture of Engineering Materials and Structures 21 (12), 1447–1457.

Martynenko, M.A., Ulitko, A.F., 1978. Stress state near the vertex of a spherical notch in an unbounded elastic medium. Soviet Applied Mechanics 14 (9), 911–918.

Mencik, J., 1996. Mechanics of Components with Treated or Coated Surfaces. Solid Mechanics and its Applications, vol. 42. Kluwer Academic Publishers, London. p. 360.

Moës, N., Gravouil, A., Belytschko, T., 2002. Non-planar 3D crack growth by the extended finite element and level sets-Part I: mechanical model. International Journal for Numerical Methods in Engineering 53 (11), 2549–2568.

Nikishkov, G.P., Atluri, S.N., 1987. Calculation of fracture mechanics parameters for an arbitrary three-dimensional crack, by the 'equivalent domain integral' method. International Journal for Numerical Methods in Engineering 24 (9), 1801–1821.

Shaghaghi, A., Ghajar, R., Alfano, M., submitted for publication. Finite element evaluation of stress intensity factors in curved non-planar cracks in FGMs.

Shaghaghi, A., Ghajar, R., Alfano, M., 2010b. An ABAQUS implementation of the isoparametric graded finite elements. Technical Report. University of Calabria (Available upon request).

Sládek, V., Sládek, J., 1983. Three-dimensional curved crack in an elastic body. International Journal of Solids and Structures 19 (5), 425–436.

Walters, M.C., Paulino, G.H., Dodds Jr., R.H., 2004. Stress-intensity factors for surface cracks in functionally graded materials under mode-I thermomechanical loading. International Journal of Solids and Structures 41 (3–4), 1081–1118.

Walters, M.C., Paulino, G.H., Dodds Jr., R.H., 2006. Computation of mixed-mode stress intensity factors for cracks in three-dimensional functionally graded solids. Journal of Engineering Mechanics 132 (1), 1–15.

Walters, M.C., Paulino, G.H., Dodds Jr., R.H., 2005. Interaction integral procedures for 3-D curved cracks including surface tractions. Engineering Fracture Mechanics 72 (11), 1635–1663.

Williams, M.L., 1957. On the stress distribution at the base of a stationary crack. ASME Journal of Applied Mechanics 24, 109–114.

Yau, J.F., Wang, S.S., Corten, H.T., 1980. A mixed-mode crack analysis of isotropic solids using conservation laws of elasticity. Journal of Applied Mechanics. 47, 335–341.

Yildirim, B., Dag, S., Erdogan, F., 2005. Three dimensional fracture analysis of FGM coatings under thermomechanical loading. International Journal of Fracture 132 (4), 369–395.

Yu, H., Wu, L., Guo, L., Wu, H., Du, S., 2010. An interaction integral method for 3D curved cracks in nonhomogeneous materials with complex interfaces. International Journal of Solids and Structures. doi:10.1016/j.ijsolstr.2010.04.027.